Clinical Radiology 74 (2019) 898.e7–898.e13

Contents lists available at ScienceDirect

Clinical Radiology

journal homepage: www.clinicalradiologyonline.net

Three-dimensional reversed fast imaging with steady-state precession diffusion-weighted imaging for the detection of middle ear cholesteatoma

Z.A. Khant [a], M. Azuma [a,*], Y. Kadota [a], Y. Hattori [a], N. Nagai [b], S. Ide [b], T. Tono [b], T. Hirai [a]

[a] Department of Radiology, Faculty of Medicine, University of Miyazaki, Miyazaki, Japan
[b] Department of Otolaryngology-Head & Neck Surgery, Faculty of Medicine, University of Miyazaki, Miyazaki, Japan

ARTICLE INFORMATION

Article history:
Received 24 April 2019
Accepted 19 July 2019

AIM: To determine the usefulness of three-dimensional reversed fast imaging with steady-state precession diffusion-weighted imaging (3D-PSIF DWI) for the detection of middle ear cholesteatoma.

MATERIALS AND METHODS: The study population consisted of 81 patients who underwent 3D-PSIF-DWI at 3 T. They included cholesteatoma in 73 cases, otitis media in five, and cholesterol granuloma in three. Two observers independently performed qualitative evaluations for the detection of cholesteatoma and measured apparent diffusion coefficient (ADC) values and ADC ratios of the lesions. Kappa (κ) statistics, the intraclass correlation coefficient (ICC), the independent *t*-test, and receiver operating characteristic (ROC) analysis were used for statistical analysis. Pair-wise comparison of the ROC curves was performed using the area under the ROC curve (AUC).

RESULTS: Interobserver agreement and ICC for the qualitative and quantitative evaluations were excellent (κ=0.92 and ICC=0.90–0.92, respectively). The ADC value and the ADC ratio were significantly lower for cholesteatoma than non-cholesteatoma lesions ($p<0.0001$). In <5 mm cholesteatoma group, the diagnostic performance of the ADC value (AUC=0.97) and the ADC ratio (AUC=1) was significantly superior to qualitative 3D-PSIF-DWI (AUC=0.76; $p=0.0001$ and <0.0001, respectively). For ≥5 mm cholesteatoma group, there were no significant differences in diagnostic performance among the three parameters.

CONCLUSION: 3D-PSIF-DWI sequence is useful for the detection of middle ear cholesteatomas, especially <5 mm lesions.

Introduction

Early detection and treatment of cholesteatomas are important to prevent their severe intra- and extracranial complications including meningitis, brain abscess, lateral

* Guarantor and correspondent: M. Azuma, Department of Radiology, Faculty of Medicine, University of Miyazaki, 5200 Kihara, Kiyotake, Miyazaki, 889-1692, Japan. Tel.: +81-985-85-2807; fax: +81-985-85-7172.
E-mail address: minako_azuma@med.miyazaki-u.ac.jp (M. Azuma).

https://doi.org/10.1016/j.crad.2019.07.013
0009-9260/

sinus thrombosis, facial nerve paralysis, and labrynthine fistula.[1] Echo-planar (EP) diffusion-weighted imaging (DWI) and non-EP-DWI techniques have been used to diagnose cholesteatomas.[2–9] Although EP-DWI has a short acquisition time, it is affected by air–bone susceptibility artefacts and distortion, which limit its diagnostic performance for cholesteatoma.[2,3]

Consequently, non-EP-DWI techniques have been increasingly used, and many studies reported their usefulness for the evaluation of cholesteatomas[2–9]; however, some investigators encountered false-positive and negative results with qualitative analysis of non-EP-DWI techniques.[7,8] Therefore, quantitative evaluation of non-EP-DWI techniques has been performed to promote their diagnostic performance.[4–6]

Three-dimensional (3D) reversed fast imaging with steady-state precession (3D-PSIF) DWI is a non-EP-DWI technique; its spatial resolution is high and artefacts are few.[10–14] It has been used to demonstrate the cranial nerves, lumbosacral plexus, peripheral nerves, intraparotid facial nerves, and parotid ducts on 3 T magnetic resonance images (MRI)[10–14]; however, the 3D-PSIF technique has not been investigated for the evaluation of cholesteatoma. Therefore, the purpose of this study was to determine the usefulness of 3D-PSIF DWI for the detection of middle ear cholesteatoma.

Materials and methods

Patient selection

This retrospective study was approved by the institutional review board, informed patient consent was waived. Data were collected from 372 consecutive patients. Between January 2012 and December 2017, all patients underwent MRI studies of the temporal bone region including axial 3D-PSIF-DWI for the evaluation of middle ear lesions.

Excluded were 291 patients for whom no axial T1, T2-weighted images (T1WI, T2WI) and apparent diffusion coefficient (ADC) maps were available, patients who underwent postoperative follow-up MRI studies for the evaluation of residual or recurrent lesions, patients without a pathological diagnosis, patients with lesions at sites other than the middle ear, and patients whose MRI examinatons showed severe motion artefacts. Consequently, 81 patients (43 males, 38 females; age range 3–73 years; mean age 35.4 years) were included. In all 81 patients, 73 patients (90.1%; 42 males, 31 females; age range 3–72 years; mean age 33.2 years) harboured cholesteatomas and the other eight patients (9.9%; one male and 7 females; age range 12–73 years; mean age 55.8 years) had non-cholesteatomas (otitis media, n=5, cholesterol granuloma, n=3).

MRI protocol

All MRI studies were performed using a 3 T MRI system (Magnetom Verio; Siemens, Erlangen, Germany); a 32-channel head coil was used. After conventional axial T1WI and T2WI, 3D-PSIF-DWI, and contrast-enhanced T1WI was undertaken. The imaging parameters for the sequences were as follows: (a) for T1WI, repetition time (TR)/echo time (TE), 600/10 ms; field of view (FOV), 150×150 mm; matrix, 192×320; section thickness/gap, 2.5/0.5 mm; voxel size, 0.78×0.47×2.5 mm^3; acquisition time, 3 minutes, 7 seconds; number of acquisitions, 2; SENSE factor, 1; (b) for T2WI, TR/TE, 4000/92 ms; FOV, 150×150 mm; matrix, 288×320; section thickness/gap, 2.5/0.5 mm; voxel size, 0.52×0.47×2.5 mm^3; acquisition time, 2 minutes, 34 seconds; number of acquisitions, 1; SENSE factor, 2; and (c) for 3D-PSIF-DWI, TR/TE, 25/2.6 ms; FOV, 220×220 mm; matrix, 192×192; section thickness/gap, 2/0.4 mm; voxel size, 1.15×1.15×2 mm^3; acquisition time, 3 minutes, 48 seconds; number of acquisitions, 2; SENSE factor, 2.

Image analysis

Qualitative evaluation

An image set was evaluated for each patient. The image set included T1WI, T2WI, 3D-PSIF-DWI, and contrast-enhanced T1WI images. The sets were shuffled and presented on a picture archiving and communication system (PACS) workstation in random order to two readers (T.H. and Z.A.K. with 29 and 3 years of experience in neuro-MRI, respectively). They were blinded to the patient identity and to clinical and pathological findings. They independently scored the confidence level for the presence or absence of cholesteatoma on a five-point scale where 1=definitely absent, 2=probably absent, 3=equivocal, 4=probably present, and 5=definitely present. T2WI and T1WI images were used for anatomical reference.

Lesions with marked and relative hyperintensity on DWI compared to brain tissue without artefacts received a score of 5 and 4, respectively, unless the same lesion was hyperintense on T1WI compared to the cerebral white matter because this phenomenon is strongly suggestive of cholesterol granuloma.[2,4] Cholesterol granulomas can be hyperintense on DWI due to the T2 shine-through effect[15] and cholesteatomas are usually hypo- or iso-intense on T1WI compared to brain tissue.[4] A score of 3 was assigned to lesions that were iso-intense on DWI compared to brain tissue or hyperintense on T1WI relative to the cerebral white matter, an observation strongly suggestive of cholesterol granuloma.[2,4,15] When a lesion was hypointense on DWI compared to brain tissue, the assigned score was 2; when there was no signal intensity on DWI, a score of 1 was recorded. When both readers assigned identical scores to the individually assessed images, the data were collected; when their initial scoring differed, the final score was recorded by consensus. Scores 4 and 5 were considered positive for the prediction of cholesteatoma.

With T1WI and T2WI guidance, one reader recorded the maximum size of the signal abnormality of the lesions on DWI on a PACS workstation. After blinded evaluations, both readers consensually identified the reason(s) for incorrect image interpretation.

Quantitative evaluation

For each patient, two observers (M.A. and Z.A.K. with 8 and 3 years of experience in neuro-MRI, respectively)

independently measured ADC values on ADC maps separately on a PACS workstation. To measure the ADC values, a circular region of interest (ROI) was drawn within the largest lesion area on DWI and then copied onto the ADC map. Using the same ROI size, they also measured the ADC value of the pons at the level of the internal auditory canal. ADC ratios were calculated with the formula:

ADC ratio=ADC value of the lesion/ADC value of the pons.

The averaged values of the ADC values and of the ADC ratios recorded by the two observers were defined as the mean ADC value and the mean ADC ratio, respectively.

Statistical analysis

Analysis for whole patient data was performed. The lesions were divided into group 1 (<5 mm) and group 2 (≥5 mm). As the number of patients with non-cholesteatoma lesions was small, they were included in both groups to evaluate diagnostic performance. All statistical analyses were performed with MedCalc statistical software (Version 18.2.1; MedCalc Software, Ostend, Belgium).

Interobserver agreement with respect to the reader-assigned scores was analysed with the kappa coefficient (κ<0.20=poor, κ=0.21–0.40=fair, κ=0.41–0.60=moderate, κ=0.61–0.80=good, κ=0.81–0.90=very good, κ>0.90=excellent agreement). To assess the reliability of the ADC measurements, the intraclass correlation coefficient (ICC) was used; ICC<0.40=poor, ICC=0.40–0.59=fair, ICC=0.60–0.74=good, and ICC>0.74=excellent. To compare the mean ADC values and the mean ADC ratios between cholesteatomas and non-cholesteatomas, the independent *t*-test we applied. Receiver operating characteristic (ROC) analysis was performed to evaluate the diagnostic performance of DWI, the ADC value and the ADC ratio and calculate their sensitivity, specificity, and accuracy. Pair-wise comparison of the ROC curves was also performed using the area under the ROC curve (AUC). Differences of $p<0.05$ were considered statistically significant.

Results

The average maximum size of the 73 cholesteatomas was 9 mm (range 2.4–35.2 mm); it was 17.7 mm (range 4.4–26.7 mm) for the eight non-cholesteatoma lesions. Subgroups included group 1 ($n=33$), 25 patients with cholesteatomas of <5 mm (mean, 3.7 mm; range, 2.4–4.9 mm) and eight non-cholesteatoma patients, and group 2 ($n=56$), 48 patients with cholesteatoma of ≥5 mm (mean, 11.3 mm; range, 5.5–35.2 mm) and the same eight non-cholesteatoma patients.

Qualitative evaluation

Interobserver agreement for qualitative evaluation was excellent for 3D-PSIF-DWI (κ=0.92; 95% confidence interval=0.86–0.97). According to the consensual final scores, 80.8% (59/73) of cholesteatoma cases had confidence scores of 4 and 5 (Fig 1), 19.2% (14/73) of cholesteatoma cases had qualitative confidence scores of 3 (Fig 2), and 100% (8/8) of non-cholesteatoma cases had qualitative confidence scores of 2 and 3 (Fig 3). The sensitivity, specificity, and accuracy of 3D-PSIF-DWI for the detection of cholesteatoma are detailed in Table 1.

Retrospective consensus review revealed the reasons for incorrect interpretation for 14 of 73 (19.2%) 3D-PSIF-DWI examinations. In 13 cholesteatoma patients (11 in group 1, two in group 2), the false-negative result of 3D-PSIF-DWI interpretation was attributable to iso-intensity (Fig 2). In one patient in group 1, the lesion determination on 3D-PSIF-DWI was false-negative due to hyperintensity on T1WI, a characteristic of cholesterol granuloma, although 3D-PSIF-DWI showed hyperintensity. 3D-PSIF-DWI returned no false-positive results; the smallest cholesteatoma detected by 3D-PSIF-DWI measured 2.4 mm.

Quantitative evaluation

The ICC with a 95% confidence interval for interobserver agreement in two quantitative parameters was excellent; it was 0.92 with 0.87–0.94 for 3D-PSIF-ADC value and 0.90 with 0.84–0.93 for 3D-PSIF-ADC ratio. The mean 3D-PSIF-ADC value and 3D-PSIF-ADC ratio were significantly lower for cholesteatomas than non-cholesteatomas ($p<0.0001$; Table 2). At a cut-off value of 1.218 (all patients and group 2) and 1.1774 (group 1), the 3D-PSIF-ADC ratio yielded the highest sensitivity, specificity, and accuracy (Table 1).

ROC analysis

Pair-wise comparison of the ROC curves and AUCs of 3D-PSIF-DWI parameters is shown in Fig 4 and Table 3, respectively. For all patients ($n=81$), the diagnostic performance of the 3D-PSIF-ADC value (AUC=0.99) and the 3D-PSIF-ADC ratio (AUC=1) was significantly higher than qualitative 3D-PSIF-DWI (AUC=0.904; $p=0.0002$ and <0.0001, respectively) although there was no significant difference between the 3D-PSIF-ADC value and the 3D-PSIF-ADC ratio ($p=0.3286$; Fig 4a).

In group 1 ($n=33$), the diagnostic performance of the 3D-PSIF-ADC value (AUC=0.97) and the 3D-PSIF-ADC ratio (AUC=1) was significantly superior to qualitative 3D-PSIF-DWI (AUC=0.76; $p=0.0001$ and <0.0001, respectively) although no significant difference was observed between the 3D-PSIF-ADC value and the 3D-PSIF-ADC ratio ($p=0.3286$; Fig 4b).

In group 2 ($n=56$), the highest diagnostic performance was obtained with the 3D-PSIF-ADC value (AUC=1) and the 3D-PSIF-ADC ratio (AUC=1), followed by the 3D-PSIF-DWI (AUC=0.979), although there were no significant differences among the three parameters (Fig 4c).

Discussion

The present study indicated that the qualitative and quantitative parameters of 3D-PSIF-DWI sequence were useful for the detection of middle ear cholesteatomas, and the use of ADC value and ratio improved the diagnostic

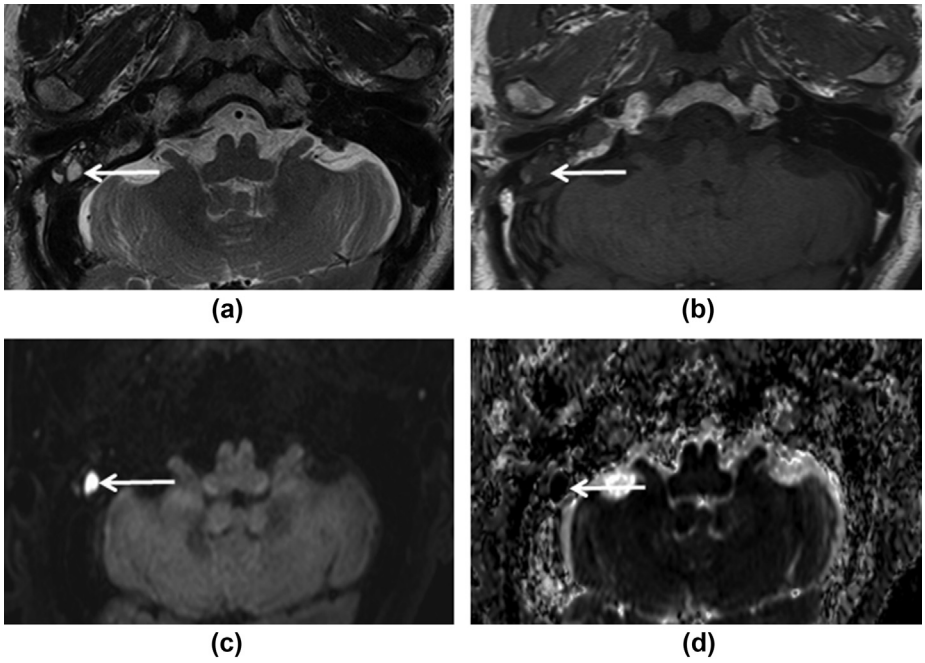

Figure 1 A 59-year-old man with a histopathologically proven 11.2-mm pars flaccida cholesteatoma in the right middle ear. Compared with the cerebellum, the lesion (arrow) is hyperintense on T2WI (a) and 3D-PSIF-DWI (c) and, hypointense on T1WI (b). Both readers agreed that the lesion was a cholesteatoma (score 5) on the 3D-PSIF-DWI. This case was true-positive by 3D-PSIF-DWI. On 3D-PSIF-ADC map (d), the mean 3D-PSIF-ADC value and ratio of the cholesteatoma were 0.25×10^{-3} mm^2/s and 0.63, respectively.

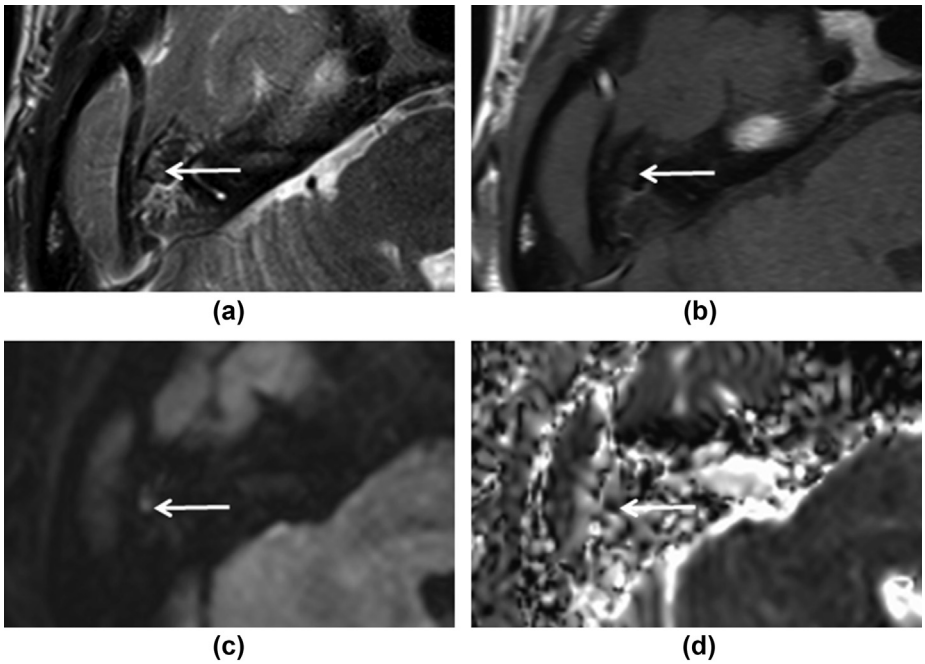

Figure 2 A 37-year-old woman with a histopathologically proven 3-mm pars flaccida cholesteatoma in the right middle ear. Compared with the cerebellum, the lesion (arrow) is iso-intense on T2WI (a) and 3D-PSIF-DWI (c) and, hypointense on T1WI (b). Both readers recorded the lesion as equivocal (score 3) on the 3D-PSIF-DWI. This case was false-negative by 3D-PSIF-DWI. On 3D-PSIF-ADC map (d), the mean 3D-PSIF-ADC value and ratio of the cholesteatoma were 0.09×10^{-3} mm^2/s and 0.21, respectively.

performance of the qualitative analysis, especially with respect to <5 mm cholesteatomas as the quantitative parameters were significantly lower in cholesteatoma than non-cholesteatoma lesions. Interobserver agreement and the ICC value were acceptable. The usefulness of 3D-PSIF-DWI is attributed to its resistance to susceptibility artefacts because it is less sensitive to heterogeneous magnetic fields.[13] In addition, chemical shift artefacts are reduced on

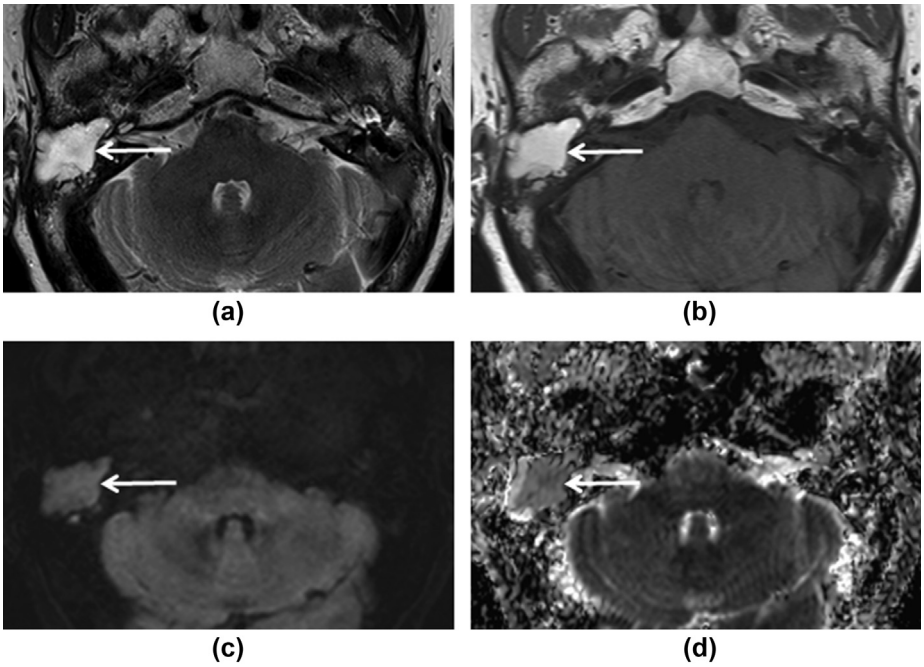

Figure 3 A 61-year-old woman with histopathologically proven cholesterol granuloma in the right middle ear. Compared with the cerebellum, the lesion (arrow) is hyperintense on T2WI (a), T1WI (b) and 3D-PSIF-ADC map (d), and iso-intense on 3D-PSIF-DWI (c). Both readers agreed that the lesion was equivocal (score 3) on the 3D-PSIF-DWI. This case was true-negative by 3D-PSIF-DWI. The mean 3D-PSIF-ADC value and ratio of the cholesterol granuloma were 0.88×10^{-3} mm^2/s and 1.69, respectively.

Table 1
Sensitivity, specificity, accuracy, and cut-off value of 3D-PSIF-DWI parameters for the diagnosis of cholesteatoma.

	Cut-off value	Sensitivity	Specificity	Accuracy
All patients group (n=81)				
Qualitative evaluation				
3D-PSIF-DWI	–	80.82%	100%	82.72%
Quantitative evaluation				
3D-PSIF-ADC value	0.695[a]	98.63%	100%	98.77%
3D-PSIF-ADC ratio	1.218	100%	100%	100%
Group 1 (n=33)[b]				
Qualitative evaluation				
3D-PSIF-DWI	–	52%	100%	63.64%
Quantitative evaluation				
3D-PSIF-ADC value	0.695[a]	96%	100%	96.97%
3D-PSIF-ADC ratio	1.1774	100%	100%	100%
Group 2 (n=56)[c]				
Qualitative evaluation				
3D-PSIF-DWI	–	95.83%	100%	96.43%
Quantitative evaluation				
3D-PSIF-ADC value	0.615[a]	100%	100%	100%
3D-PSIF-ADC ratio	1.218	100%	100%	100%

[a] ADC values are presented as $\times10^{-3}$ mm^2/s.
[b] Group 1: 25 patients with cholesteatoma <5 mm and the eight non-cholesteatoma patients.
[c] Group 2: 48 patients with cholesteatoma ≥5 mm and the same eight non-cholesteatoma patients.

3D-PSIF-DWI because water-excitation and fat-suppression techniques are implemented simultaneously.[13] Lastly, 3D-PSIF-DWI involves 3D Fourier-encoding and high spatial resolution, resulting in the clear visualisation of anatomic details.[13] Although 3D-PSIF-DWI has been performed for the visualisation of the nerves, lumbosacral plexus, and parotid ducts,[10–14] there are no reports on its application for the evaluation of cholesteatoma.

The qualitative diagnostic performance of non-EP-DWI for the detection of cholesteatomas has been investigated. One earlier half-Fourier single-shot turbo spin-echo (HASTE) DWI study on 44 patients revealed that their sensitivity and specificity were 55% and 71%, respectively.[7] Locketz *et al.*[8] demonstrated that in their 12 patients, the sensitivity and specificity of periodically rotated overlapping parallel lines with enhanced reconstruction (PROPELLER) DWI were 75%. We found that the sensitivity of qualitative 3D-PSIF-DWI was 80.8% for all patients, 52% for group 1 (<5 mm), and 95.8% for group 2 (≥5 mm); overall specificity was 100%. Unlike the present study, the earlier studies did not include patients with non-cholesteatoma lesions, such as otitis media and cholesterol granuloma. In addition, they did not evaluate the size of the cholesteatomas, and the study populations were smaller than the

Table 2
Mean 3D-PSIF-ADC values and ratios.

	Cholesteatoma (n=73)	Non-cholesteatoma (n=8)	p-Value
3D-PSIF-ADC value[a]	0.3318±0.1568 (0.085–1.03)	0.9563±0.1721 (0.7–1.25)	<0.0001
3D-PSIF-ADC ratio	0.7116±0.2516 (0.2078–1.218)	2.2425±0.4426 (1.6526–2.838)	<0.0001

Data in parentheses show the range. Values are the mean±standard deviation; they are compared using the independent t-test.
[a] ADC values are presented as $\times10^{-3}$ mm^2/s.

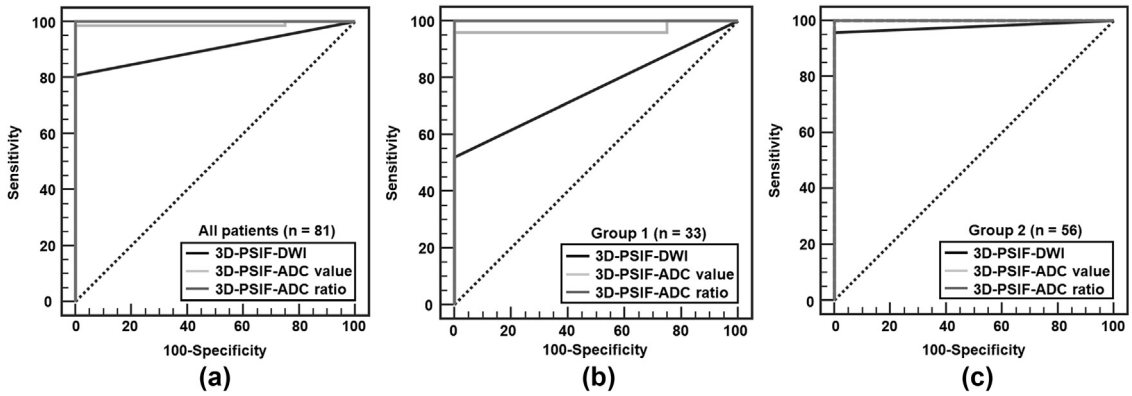

Figure 4 ROC curves of 3D-PSIF-DWI parameters and comparison of the ROC curves for all 81 patients (a), group 1 (b), and group 2 (c). Group 1 includes 25 patients with cholesteatoma measuring <5 mm and the eight non-cholesteatoma patients. Group 2 includes 48 patients with cholesteatoma ≥5 mm and also the same eight non-cholesteatoma patients.

Table 3
Comparison of AUCs of 3D-PSIF-DWI parameters.

	AUC	*p*-Value
All patients group (*n*=81)		
3D-PSIF-DWI vs 3D-PSIF-ADC value	0.904 (0.818–0.958) vs 0.99 (0.937–1.0)	0.0002
3D-PSIF-DWI vs 3D-PSIF-ADC ratio	0.904 (0.818–0.958) vs 1.0 (0.955–1.0)	<0.0001
3D-PSIF-ADC value vs 3D-PSIF-ADC ratio	0.99 (0.937–1.0) vs 1.0 (0.955–1.0)	0.3286
Group 1 (*n*=33)[a]		
3D-PSIF-DWI vs 3D-PSIF-ADC value	0.76 (0.58–0.891) vs 0.97 (0.843–0.999)	0.0001
3D-PSIF-DWI vs 3D-PSIF-ADC ratio	0.76 (0.58–0.891) vs 1.0 (0.894–1.0)	<0.0001
3D-PSIF-ADC value vs 3D-PSIF-ADC ratio	0.97 (0.843–0.999) vs 1.0 (0.894–1.0)	0.3286
Group 2 (*n*=56)[b]		
3D-PSIF-DWI vs 3D-PSIF-ADC value	0.979 (0.9–0.999) vs 1.0 (0.936–1.0)	0.1529
3D-PSIF-DWI vs 3D-PSIF-ADC ratio	0.979 (0.9–0.999) vs 1.0 (0.936–1.0)	0.1529
3D-PSIF-ADC value vs 3D-PSIF-ADC ratio	1.0 (0.936–1.0) vs 1.0 (0.936–1.0)	1.0

All patients group (*n*=81).
[a] Group 1: 25 patients with cholesteatoma <5 mm and the eight non-cholesteatoma patients.
[b] Group 2: 48 patients with cholesteatoma ≥5 mm and the same eight non-cholesteatoma patients.

present study. Thus, it is difficult to compare the results between the present and previous reports; however, the results of the present are in accordance with a meta-analysis containing 16 non-EP-DWI studies because their results demonstrated that the sensitivity and specificity were 89.8% and 94.6%.[3]

3D-PSIF-DWI resulted in false-negative readings particularly in patients with <5 mm cholesteatoma; their DWI revealed iso-intensity. The lack of necessary keratin in the cholesteatoma may account for this observation.[5,9] Other false-negative cholesteatoma results were attributable to their exhibiting hyperintensity on T1WI. This observation also applies to cholesterol granulomas that may be hyperintense on DWI due to T2 shine-through effects.[2,4,15] The smallest cholesteatoma detected in the present study on 3D-PSIF-DWI measured 2.4 mm. Others identified cholesteatomas as small as 2 mm on non-EP-DWI sequences.[15]

The usefulness of quantitative ADC measurements of non-EP-DWI in patients with cholesteatoma has been reported. Lingam *et al.*[5] demonstrated that in their 67 patients, the HASTE-ADC value manifested 100% sensitivity and 96% specificity; however, they did not evaluate the size of the cholesteatomas. In addition, they excluded four patients with cholesteatomas <3 mm because the ADC values could not be calculated. Another study[4] that recorded the TSE-ADC values of 57 patients found that the sensitivity and specificity were 97% and 89%, respectively; however, the study population was relatively small and the cholesteatomas were large (4–30 mm). Recently, Cavaliere *et al.*[6] reported that in 109 patients, the ADC value of multishot non-EP-DWI yielded 97% sensitivity and 100% specificity; however, they did not mention the size of the cholesteatomas. Cholesteatomas could be diagnosed based on the 3D-PSIF-ADC value at a sensitivity of 98.63% and a specificity of 100% with a cut-off value of 0.695 when all 81 patients were evaluated in the present study. When they were separated into those with lesions <5 mm (group 1) and those whose lesions were ≥5 mm (group 2), the sensitivity and specificity were 96% and 100% with a cut-off value of 0.695, respectively, in group 1, and 100% and 100% with a cut-off value of 0.615 in group 2. Although the evaluation method using the ADC ratio was not applied in earlier studies, the diagnostic performance of the ADC ratio was as high as that of the 3D-PSIF-ADC value. Therefore, quantitative parameters, such as the ADC value and the ADC ratio, reduced the false-negative results of qualitative 3D-PSIF-DWI evaluation, especially in the <5

mm cholesteatomas showing iso-intensity on DWI. 3D-PSIF-DWI is recommended for the diagnosis of middle ear cholesteatoma.

In the present study, the acquisition time of 3D-PSIF-DWI was 3 minutes 48 seconds. In other non-EP-DWI studies for cholesteatoma, the acquisition time was 2 minutes 40 seconds for 3D turbo field-echo with diffusion-sensitised driven-equilibrium preparation (TFE-DSDE) DWI, 2 minutes 34 seconds for PROPELLER-DWI and 4 minutes 15 seconds for HASTE-DWI.[2,8,16] Although the acquisition time of 3D-PSIF-DWI was relatively longer than 3D-TFE-DSDE-DWI and PROPELLER-DWI, and relatively shorter than HASTE-DWI, it was not largely different from the other non-EP-DWI sequences.

The present study has some limitations. The eight non-cholesteatoma patients were included in both group 1 and group 2 to evaluate diagnostic performance. As few patients with non-cholesteatomas are candidates for surgery further patients could not be recruited. In addition, only the 3D-PSIF-DWI sequence was performed and other non-EP-DWI sequences were not included.

In conclusion, the 3D-PSIF-DWI sequence is useful for the detection of middle ear cholesteatomas. As the use of quantitative parameters, such as the ADC value and the ADC ratio, increased the diagnostic performance of the 3D-PSIF-DWI sequence, especially in patients with lesions <5 mm, quantitative evaluation for the diagnosis of middle ear cholesteatomas is recommended.

Conflicts of interest

The authors declare no conflict of interest.

References

1. Prasad SC, Shin SH, Russo A, *et al*. Current trends in the management of the complications of chronic otitis media with cholesteatoma. *Curr Opin Otolaryngol Head Neck Surg* 2013;**21**:446–54.
2. Yamashita K, Yoshiura T, Hiwatashi A, *et al*. High-resolution three-dimensional diffusion-weighted imaging of middle ear cholesteatoma at 3.0 T MRI: usefulness of 3D turbo field-echo with diffusion-sensitised driven-equilibrium preparation (TFE-DSDE) compared to single-shot echo-planar imaging. *Eur J Radiol* 2013;**82**:e471–5.
3. Muzaffar J, Metcalfe C, Colley S, *et al*. Diffusion-weighted magnetic resonance imaging for residual and recurrent cholesteatoma: a systematic review and meta-analysis. *Clin Otolaryngol* 2017;**42**:536–43.
4. Özgen B, Bulut E, Dolgun A, *et al*. Accuracy of turbo spin-echo diffusion-weighted imaging signal intensity measurements for the diagnosis of cholesteatoma. *Diagn Interv Radiol* 2017;**23**:300–6.
5. Lingam RK, Khatri P, Hughes J, *et al*. Apparent diffusion coefficients for detection of postoperative middle ear cholesteatoma on non-echo-planar diffusion-weighted images. *Radiology* 2013;**269**:504–10.
6. Cavaliere M, Di Lullo AM, Cantone E, *et al*. Cholesteatoma vs granulation tissue: a differential diagnosis by DWI-MRI apparent diffusion coefficient. *Eur Arch Otorhinolaryngol* 2018;**275**:2237–43.
7. Nash R, Lingam RK, Chandrasekharan D, *et al*. Does non-echo-planar diffusion-weighted magnetic resonance imaging have a role in assisting the clinical diagnosis of cholesteatoma in selected cases? *J Laryngol Otol* 2018;**132**:207–13.
8. Locketz GD, Li PM, Fischbein NJ, *et al*. Fusion of computed tomography and PROPELLER diffusion-weighted magnetic resonance imaging for the detection and localization of middle ear cholesteatoma. *JAMA Otolaryngol Head Neck Surg* 2016;**142**:947–53.
9. Lingam RK, Nash R, Majithia A, *et al*. Non-echoplanar diffusion weighted imaging in the detection of post-operative middle ear cholesteatoma: navigating beyond the pitfalls to find the pearl. *Insights Imaging* 2016;**7**:669–78.
10. Zhang Z, Meng Q, Chen Y, *et al*. 3-T imaging of the cranial nerves using three-dimensional reversed FISP with diffusion-weighted MR sequence. *J Magn Reson Imaging* 2008;**27**:454–8.
11. Zhang ZW, Song LJ, Meng QF, *et al*. High-resolution diffusion-weighted MR imaging of the human lumbosacral plexus and its branches based on a steady-state free precession imaging technique at 3T. *AJNR Am J Neuroradiol* 2008;**29**:1092–4.
12. Zare M, Faeghi F, Hosseini A, *et al*. Comparison between three-dimensional diffusion-weighted PSIF technique and routine imaging sequences in evaluation of peripheral nerves in healthy people. *Basic Clin Neurosci* 2018;**9**:65–71.
13. Chu J, Zhou Z, Hong G, *et al*. High-resolution MRI of the intraparotid facial nerve based on a microsurface coil and a 3D reversed fast imaging with steady-state precession DWI sequence at 3T. *AJNR Am J Neuroradiol* 2013;**34**:1643–8.
14. Naganawa S, Ishihara S, Satake H, *et al*. Simultaneous three-dimensional visualization of the intra-parotid facial nerve and parotid duct using a three-dimensional reversed FISP sequence with diffusion weighting. *Magn Reson Med Sci* 2010;**9**:153–8.
15. De Foer B, Vercruysse JP, Spaepen M, *et al*. Diffusion-weighted magnetic resonance imaging of the temporal bone. *Neuroradiol* 2010;**52**:785–807.
16. Ilıca AT, Hıdır Y, Bulakbaşı N, *et al*. HASTE diffusion-weighted MRI for the reliable detection of cholesteatoma. *Diagn Interv Radiol* 2012;**18**:153–8.